Enhanced corrosion inhibition of carbon steel in HCl solution by a newly synthesized hydrazone derivative: Mechanism exploration from electrochemical, XPS, and computational studies

O.M.A. Khamaysa, I. Selatnia, H. Zeghache, Hassane Lgaz, Assia Sid, I.-M. Chung, M. Benahmed, Noureddine Gherraf, Paul Mosset

HAL Id: hal-02932008
https://hal.science/hal-02932008

Submitted on 11 Sep 2020

Enhanced Corrosion Inhibition of Carbon Steel in HCl Solution by a Newly Synthesized Hydrazone Derivative: Mechanism Exploration from Electrochemical, XPS, and Computational Studies

Oday Mohammad Ahmad Khamaysa[1], Ilhem Selatnia[1], Hadjer Zeghache[2], Hassane Lgaz[3*], Assia Sid[1], Ill-Min Chung[3], Merzoug Benahmed[4], Noureddine Gherraf[5], and Paul Mosset[6]

"[1]Laboratory of Analytical Sciences, Materials and Environmental (LSAME). Larbi Ben M'Hidi University. Oum El Bouaghi. 04000. Algeria.
[2]Laboratory of Applied Chemistry and Material Technology (LCATM). Material Structure Departement. Larbi Ben M'Hidi University. Oum El Bouaghi. 04000. Algeria.
[3]Department of Crop Science, College of Sanghur Life Science, Konkuk University, Seoul 05029, South Korea.
[4]Laboratory of Bioactive Molecules and Applications. Tebessa University, Route de Constantine, Tebessa, 12000 Algeria.
[5]Laboratory des Ressources Naturelles et Aménagement des Milieux Sensibles, Larbi ben M'Hidi University, Oum El Bouaghi, Algeria.
[6]Université de Rennes 1, Institut des Sciences Chimiques de Rennes, CNRS UMR 6226, Avenue du Général Leclerc, 35042 Rennes Cedex, France.

*Corresponding authors:

Hassane Lgaz, Email: hlgaz@konkuk.ac.kr ; **Oday Mohammad Ahmad Khamaysa**

Email: khamaysa.oday@univ-oeb.dz"

Abstract

The corrosion inhibition properties of a synthesized hydrazone derivative namely, 1-(4-isopropyl phenyl) -2- (2,4-dinitrophenyl) (HYD (*iso*)) on API 5L-X60 carbon steel (CS) in 1.0 M HCl solution were evaluated by chemical, electrochemical, X-ray photoelectron spectroscopy (XPS) and theoretical studies. The obtained results revealed that the tested compound acted as a good corrosion inhibitor with inhibition

1

efficiency of 96.32% at a concentration of 5×10^{-3} M. The polarization technique indicated that the HYD (*iso*) belonged to mixed-type inhibitors, preventing simultaneously anodic and cathodic reactions. The binding between the HYD (iso)'s molecule and CS surface follows a Langmuir adsorption type model and its inhibition mechanism is assisted by physical and chemical interactions. Scanning electron microscope (SEM) and contact angle analyses were performed to examine the surface morphology of inhibited and uninhibited samples. Additionally, theoretical studies using Density Functional Theory (DFT) and molecular dynamics (MD) simulation were performed to explore the most reactive sites of the hydrazone molecule and its adsorption mechanism.

1. Introduction

Metals and their alloys play an important role in our daily lives; they are extensively used in domestic life, numerous technological and industrial applications [1,2]. However, these materials are very prone to undergo corrosion when exposed to aggressive environments, especially those containing SO_4^{2-} and Cl^- anions, leading to damage of equipment, deterioration of surface, and append a huge economic loss [3–5]. Numerous methods were used to moderate this problem, among them, the application of corrosion inhibitors has been the most effective processes to enhance the resistance of these materials and control the damage caused by corrosion [6]. The utmost frequently used corrosion inhibitors are organic compounds, comprising moieties with π and non-bonding electrons, heteroatoms (N, O, S,....) and/or polar

functional groups [7,8], which are of paramount importance during adsorption process of inhibitors on metal surfaces [9,10]. Over the years, a vast variety of organic compounds has been tested, especially those including nitrogen "N" such as azine derivatives [11], amino acids [12], imines [13], Schiff bases [14], aminobenzonitrile [15] and hydrazine [16]. Hydrazone and its derivatives are azomethines characterized by the presence of the triatomic grouping >C=N-N<, which represent an important family of organic compounds possessing a wide variety of properties due to their both hard and soft base characters [17]. The azomethine group –NHN=CH– in hydrazones is highly reactive, where the two nitrogen atoms have nucleophilic nature and the carbon atom has both electrophilic and nucleophilic characters. Due to these promising features, hydrazones are recently getting more and more interest as corrosion inhibitors [18–21]. Therefore, we have chosen to investigate the potential of a hydrazone derivative to be a potent inhibitor against corrosion of steel in acidic solution. Traditionally, the evaluation of inhibition performance is performed experimentally using several chemical and electrochemical methods. However, it is difficult to unveil the exact mechanism that takes place between metal surface and inhibitor molecule using only these experimental methods. Recently, computational chemistry methods have emerged as a powerful tool in the field of corrosion inhibition to provide more detailed information to investigate the mechanism of inhibition at the atomic scale [22–26].

In this effort, the corrosion inhibition performance of 1-(4-isopropylphenyl) -2-(2,4-dinitrophenyl) hydrazone for CS in 1.0 M HCl was evaluated by means of several chemical and electrochemical techniques. The potential formation of a protective layer and chemical states of the CS surface were discussed through contact angle, X- ray photoelectron spectroscopy (XPS) and SEM analyses. Besides, important

theoretical insights were generated from DFT computations and molecular dynamics (MD) simulations, which shed more light on inhibitor-iron interactions.

2. Experimental

2. 1. Materials and sample preparation

Carbon steel (API 5L-X60) samples with chemical composition of (in wt.%): C (0.26), Mn (1.35), P(0.03), S (0.03) and the rest Fe were obtained from petroleum storage tanks (Algeria). Rectangular pieces with the same size ($1 \times 1 \times 1 cm^3$) were used for all measurements. The CS specimens were treated according to the ASTM G1-03 standard method [27]. The acidic environment is a 1.0 M HCl solution. After preliminary tests, the concentration range of the studied inhibitor was fixed between 10^{-4} and 5×10^{-3} M.

2. 2. Synthesis of inhibitor

(*E*) -1- (2,4-dinitrophenyl) -2- (4-isopropyl benzylidene) hydrazone (3) HYD (*iso*) used as a corrosion inhibitor was obtained as red crystals with 85 % yield through equimolar condensation between DNPH (1) and isopropyl benzaldehyde (2) in an acid medium (Ethanol / H_2SO_4 (3 drops)) during 4 hours of stirring under reflux (Scheme 1). A full spectral analysis is represented in supplementary information.
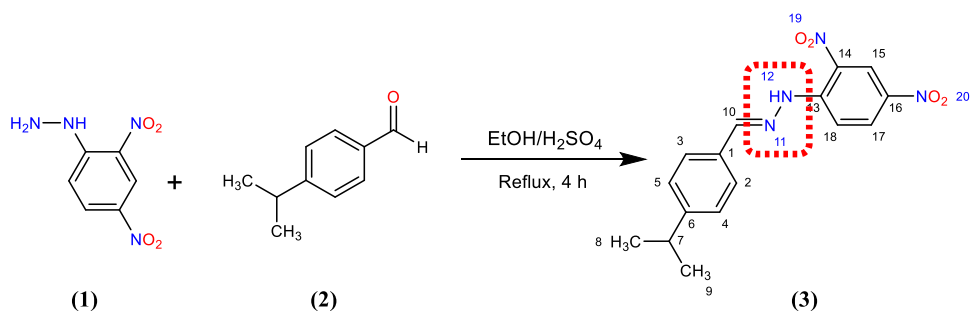
Scheme 1. Schematic representation of the synthetic pathway for the tested inhibitor HYD (*iso).*

2. 3. Weight loss and electrochemical measurements

ASTM G 31-72 standard laboratory methodology was adopted to realize the weight loss measurement [28]. The CS specimens were immersed for 2 hours in blank and inhibited solution at different temperatures ranging from 298 to 328 K. After the required time, CS coupons were retrieved from test solutions, and corrosion products were removed by a pickling acid solution, then cleaned with distilled water, followed by an acetone wash, and dried before re-weighting them again. Following equations were used to estimate the corrosion inhibition performance of the used inhibitor [29,30]:

Corrosion rate (C_R): $C_R = \frac{w}{A.t}$ (1)

The inhibition efficiency ($\eta_w\%$): $\eta_w\% = \frac{C_R^0 - C_R}{C_R^0} \times 100$ (2)

The surface coverage (θ) $\theta = \frac{\eta_w\%}{100}$ (3)

Where w is the average weight loss (g), A is the surface area of CS in cm², and t is the exposure time in hour. C_R^0 and C_R are respectively the values of corrosion rate in blank and inhibited solutions.

The electrochemical experiment were done a three-electrode system connected to Voltalab instrument (model PGZ 301) and monitored by Voltamaster 4 software. The three electrodes of the used electrochemical cell are: The CS as a working electrode (surface area of 1cm²), a platinum wire as auxiliary electrode, and saturated calomel electrode (SCE) as the reference electrode. To achieve the stabilization of the system, the CS working electrode was immersed in the test solution for 30 min at open circuit potential (E_{ocp}). After that, electrochemical impedance spectroscopy (EIS) was conducted in a frequency range from 100 KHz to 0.01 Hz with a signal

amplitude perturbation of 10 mV. The EC-Lab software was used for simulation and fitting of EIS data, and polarization resistances were used to estimate the inhibition efficiency [31]:

$$\eta_R\% = \frac{R_p - R_p^0}{R_p}.100 \qquad (4)$$

where R_p^0 and R_p are polarization resistances in the absence and presence of the inhibitor, respectively.

Potentiodynamic polarization curves were obtained by sweeping the electrode potential ± 250 mV versus E_{ocp} with a scan rate of 1 mV/s. Inhibition efficiency ($\eta_p\%$) was defined as below [32,33]:

$$\eta_p(\%) = \frac{i_{corr}^0 - i_{corr}}{i_{corr}^0}.100 \qquad (5)$$

where i_{corr}^0 and i_{corr} are the corrosion current–densities in blank and inhibited solutions, respectively.

Each test was carried out in triplicate.

2. 4. Computational details

2. 4. 1. Quantum chemical calculations

For the DFT study, HYD (*iso*) was geometrically optimized using Generalized gradient approximation (GGA) with double numerical basis sets plus polarization (DNP) [34] in aqueous solution (COSMO solvation model) [35]. All calculations were performed using the Material studio program [36]. The convergence thresholds for energy, maximum force, and maximum atomic displacement were of 1×10^{-5} Ha, 2×10^{-3} Ha Å^{-1}, and 5×10^{-3} Å, respectively, and the quality of optimization was set at fine. Various quantum chemical parameters such as E_{HOMO}, E_{LUMO}, the energy gap (

Δ), the fraction of electron transferred (ΔN) and Fukui indices were obtained from different equations described in Supplementary Material.

2. 4. 2. Molecular dynamics simulation

Recently, molecular dynamics (MD) simulation became a popular technique in the field of corrosion inhibition, shading more light on the adsorption behavior of inhibitor molecules [31,37,38]. The adsorption behavior of HYD (*iso*) on the iron surface and in the presence of water molecules and HCl was investigated by performing MD simulations using the visualizer, amorphous cell and discover modules implemented in Materials Studio from Accelrys Inc [36]. The Fe (110) system is picked up in the present study because it is the most stable among three common Fe substrates [31]. Non-bonding, van der Waals and electrostatic interactions were set as atom-based summations using the Ewald summation method with a cutoff radius of 15.5 Å. More details about the simulation procedure and the calculation of interaction and binding energy between the inhibitor molecule and Fe (110) were reported in another works [11,39–42].

2. 5. SEM and contact angle analyses

The surface analysis of corroded and inhibited CS samples was studied using QUANTA FEG250 scanning electron microscope instrument. The static contact angle values were recorded on the CS samples exposed to the uninhibited and inhibited solution by the DSA100 Kruss instrument.

2. 6. XPS Measurements

The X-ray photoelectron spectroscopy is a sensitive tool to probe the chemistry of materials. To this end, elemental analysis and characterization of the CS surface were performed by XPS measurements. Measurements were done on a Kratos Axis Ultra DLD spectrometer employing the following conditions: an analyzer pass energy of 20 kV, with a total energy resolution of 0.9 eV, and Al-Kα X-ray source (hν = 1486.6 eV).

3. Results and discussion

3.1. Weight loss: Influence of inhibitor concentration and temperature

Table 1 and Figure 1 represent the variation in the effectiveness of the investigated inhibitor molecule towards CS acidic dissolution with their concentrations. It is clear from Figure 1a that the presence of HYD (*iso*) decreases the dissolution of the steel samples, meanwhile the inhibition performance reaches a maximum value of 96.32% in the presence of 5×10^{-3} M of HYD (iso) at 298 K, which reflects its excellent corrosion inhibition properties. This phenomenon is attributed to the coverage of the metal surface by the accumulation of more number of molecules leading to the formation of an adsorbed film from HYD (*iso*) compound, and therefore, isolating it from the corrosive solution [31]. Considering the effect of temperatures, results in Table 1 reveals an increase in the corrosion rate of CS samples immersed in blank and inhibited solutions with a rise in temperature, suggesting a decline in the strength of adsorption of HYD (*iso*) molecules at higher temperatures. We also note that the inhibition efficiency decreases from 96.32% (at 298 K) to 91.25 % (at 328 K) (*via*

Figure 1b). This slight decrease confirms that the tested compound acts as an efficient inhibitor at higher temperatures. Activation parameters are provided with their discussion in Supplementary data.

Table 1. Weight loss results of differents concentrations of HYD (*iso*) in 1.0 M HCl at different temperatures for 2 hours.

Temperature (K)	C (M)	C_R (mg cm^{-2} h^{-1})	η_w (%)	θ
298	Blank	1.3210±0.1055	-	-
	1×10^{-4}	0.1247±0.0082	90.56	0.9056
	5×10^{-4}	0.0919±0.0670	93.12	0.9312
	1×10^{-3}	0.0792±0.0032	94.00	0.9400
	5×10^{-3}	0.0486±0.0016	96.32	0.9632
308	Blank	1.9521±0.1241	-	-
	1×10^{-4}	0.2323±0.0099	88.10	0.8810
	5×10^{-4}	0.1566±0.0029	91.98	0.9198
	1×10^{-3}	0.1435±0.0033	92.65	0.9265
	5×10^{-3}	0.0957±0.0042	95.10	0.9510
318	Blank	2.5744±0.0854	-	-
	1×10^{-4}	0.3403±0.0077	86.78	0.8678
	5×10^{-4}	0.3007±0.0050	88.32	0.8832
	1×10^{-3}	0.2260±0.0155	91.22	0.9122
	5×10^{-3}	0.1738±0.0015	93.25	0.9325
328	Blank	3.1423±0.0074	-	-
	1×10^{-4}	0.4792±0.0036	84.75	0.8475
	5×10^{-4}	0.4336±0.0051	86.20	0.8620
	1×10^{-3}	0.3733±0.0011	88.12	0.8812
	5×10^{-3}	0.2750±0.0049	91.25	0.9125

3. 2. Surface analysis by XPS

XPS is a useful tool to probe the chemistry of the organic inhibitor layer formed on the CS surface, which can be crucial in unveiling the adsorption mechanism of HYD (*iso*) on CS. Measurements were done on the carbon steel surface after its

9

immersion in 1.0 M HCl solution containing 5×10^{-3} M of the hydrazone derivative. The obtained XPS spectra and the high-resolution spectra of C 1s, O 1s, N 1s, and Fe 2p signals and their deconvolutions are given in Figures 2 and 3. The appearance of peaks of N and O in protected sample surface spectra (Figure 2) confirms the adsorption of HYD (*iso*) on the iron surface.

The C 1s spectrum (Figure 3a) shows three peaks at 284, 286 and 288 eV. The first peak has the major influence and corresponds to C-C, C-H of aromatic bonds and C=C [43,44]. The second peak confirms the presence of the C-N and C=N bonds [45]. The last peak may be ascribed to the carbon atom of the $C=N^+$ [46].

The deconvolution of O 1s high-resolution spectra in Figure 3b gives three components. The first peak located at lower binding energy (530.6 eV) can be attributed to O^{2-}, and could also be linked to oxygen atoms in Fe_2O_3 and/or Fe_3O_4 oxides bonded to Fe^{3+} [47]. The small peak located at around 532.2 eV possibly originates from hydroxyl oxygen –OH of iron oxides, such as FeOOH and/or $Fe(OH)_3$ [48].

A single peak is observed in the N 1s spectra (Figure 3c) at binding energy ~399 eV is attributed to N-Fe, due to the coordination of the nitrogen atom in the hydrazone moiety with the iron atom of the steel surface [44].

The deconvolution of Fe 2p may be fitted into four main peaks (Figure 3d). The first peak located at ~711eV confirms the presence of complexes of ferric ion such as Fe_2O_3 (i.e., Fe^{3+} oxide) and/or Fe_3O_4 (i.e., Fe^{2+}/Fe^{3+} mixed oxide) and FeOOH (i.e., oxy-hydroxide). Based on the oxidation state in the literature [49], the second peak located at ~ 712 eV is associated to ferryl ions Fe^{+4}, which can lead to the formation of an oxoiron (IV) complex (Scheme 2) [49,50], while the peak observed at ~ 715.63

eV is assigned to the satellite of Fe(III). XPS results confirm the effective adsorption of HYD (*iso*) molecules and how they interact with CS surface.
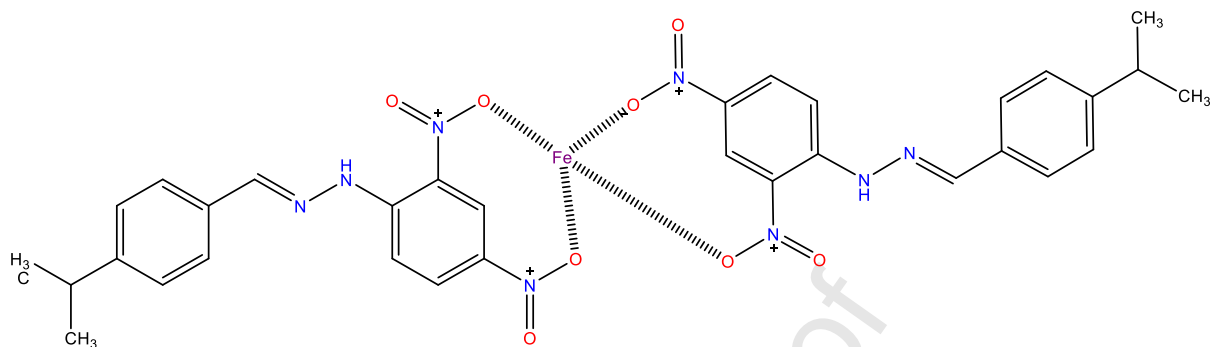
Scheme 2. The formation of an oxoiron (IV) complex.

3. 3. Electrochemical measurements

3. 3.1. EIS measurments

The CS/ HCl medium interface in the absence and presence of HYD (*iso*) at different concentrations were investigated by EIS measurement at 298 K. The obtained results are presented in Figure 4 (a, b and c). In Nyquist plots (Figure 4a), a single depressed semi-circle similar in shape for both uninhibited and inhibited solution is observed, and its diameter increases with increasing inhibitor concentration, indicating that the HYD (*iso)* molecules adsorbed at the CS/electrolyte interface without changing the corrosion mechanism and the inhibition behavior is controlled by the charge transfer process [51]. On the other hand, the imperfection of semicircle refers to the frequency dispersion, which usually results from the roughness and heterogeneity of the metal surface [52]. In the bode plots (Figure 4b,c), it is observed that, over a wide spectrum of frequencies, only one-time constant is observed. Such

11

behavior is interpreted as due to a relaxation effect resulting from inhibitor's adsorption on steel surface [53]. The increase in the low-frequency impedance modulation values (Figure 4b) is also attributed to the adsorption of HYD (*iso*) molecules on the CS surface [54]. Moreover, the obvious increase in the phase angle value from 65° in the blank solution to 74° in the presence of $5{\times}10^{-3}$M of HYD (*iso*) can be attributed to the formation of a protective layer on the CS surface.

In order to analyze the experimental results, an electrical equivalent circuit model (EEC) was employed (Figure 4d), which consists of a polarization resistance (R_p), a constant phase element (CPE), and a solution resistance (R_s). The parameters obtained by fitting the impedance spectra are listed in Table 2. The constant phase element (CPE) was employed instead of a pure capacitor, which is affected by imperfections of the surface, and its impedance is described by the following expression [39]:

$$Z_{CPE} = \frac{1}{Q(j\omega)^n} \qquad (17)$$

Where Q is the magnitude of the CPE; *j* is the imaginary number; ω is the angular frequency; *n* is the deviation parameter ($-1 \le n \le 1$), which characterizes the properties of CPE. The equation 18 is used to calculate the value of the double layer capacitance (C_{dl}) [39]:

$$C_{dl} = (Q\,R_{ct}^{1-n})^{\frac{1}{n}} \qquad (18)$$

According to results reported in Table 2, as the inhibitor concentration increase, its accumulated molecules at the metal/solution interface will adsorb at the inner Helmholtz plane, replacing water molecules. As a consequence, the double layer thickness increases and C_{dl} values decrease, which help blocking the active sites for corrosive dissolution, thus forming a protective layer against acid attack.

Table 2. Impedance parameters and inhibition efficiency values for carbon steel in 1.0 M HCl solution containing different concentrations of HYD (*iso*) at 298 K.

Inhibitor	C (M)	R_p (Ω cm^2)	R_s (Ω cm^2)	10^{-3} Q (F S^{-1})	n	C_{dl} (μF cm^{-2})	η_R(%)
	Blank	24.37±1.62	0.271±0.040	0.893	0.963	522.3±4.2	-
	1×10^{-4}	306.3±3.10	0.325±0.017	0.619	0.990	519.5±1.7	92.04
HYD (*iso*)	5×10^{-4}	335.0±2.74	0.174±0.036	0.559	0.992	475.0±2.3	92.73
	1×10^{-3}	372.9±1.93	0.345±0.010	0.520	0.993	426.7±1.3	93.46
	5×10^{-3}	767.5±1.65	0.220±0.024	0.328	0.997	261.2±2.5	96.82

3.3.2. Potentiodynamic polarization curves

The Potentiodynamic polarization curves for CS in hydrochloric acid in the absence and presence of different concentrations of HYD (*iso*) are shown in Figure 5. The corrosion parameters such as corrosion potential (E_{corr}), corrosion current density (i_{corr}), anodic and cathodic Tafel slopes (β_a and β_c) and the inhibition efficiency (η_p%) were listed in Table 3. As can be observed from Figure 5, the presence of the HYD (*iso*) shifts slightly the corrosion potential to the anodic direction and retarded both hydrogen evolution and metal dissolution reactions. Also, we noted that the values of E_{corr} did not vary drastically and the displacement is less than 85mV relating to the potential of the blank solution (*via* Table 3), reflecting mixed cathodic/ anodic inhibition effect of the tested inhibitor [51]. Moreover, corrosion current density (i_{corr}) values decreased and the inhibition efficiency increased with the addition of HYD (*iso*), due to the adsorption of inhibitor's molecules on CS surface, which blocks the active sites [55]. The higher inhibition efficiency marked in the presence of different concentrations of HYD (*iso*), i.e., 90-95%, might be due to the high electron densities

on the molecule resulting from the presence of π-electrons in the aromatic ring and lone pair electrons.

Table 3. Polarization parameters and the inhibition efficiency of carbon steel corrosion in 1.0 M HCl medium without and with different concentrations of HYD (*iso*) at 298 K.

Compound	C (M)	$-E_{corr}$ (mV/SCE)	i_{corr} (mA cm^{-2})	β_a (mV dec^{-1})	$-\beta_c$ (mV dec^{-1})	$\eta_P(\%)$
HYD (*iso*)	Blank	454.0±3.5	1.2268±0.0012	107.4±1.6	143.8±2.1	-
	1×10^{-4}	449.7±2.3	0.1158±0.0011	95.2±0.8	115.8±1.9	90.56
	5×10^{-4}	442.6±1.9	0.0927±0.0019	51.1±1.7	115.7±1.3	92.44
	1×10^{-3}	447.1±3.7	0.0719±0.0024	67.3±2.4	109.3±3.0	94.13
	5×10^{-3}	438.7±1.5	0.0512±0.0035	48.9±1.1	122.8±2.7	95.82

3.4. Adsorption isotherm

For further information about the adsorption process of HYD (*iso*) molecules onto the metal surface as well as thermodynamic parameters, several adsorption isotherm models were used to fit the experimental data (Langmuir, Temkin, and Frumkin…etc.). Langmuir adsorption isotherm model (Eq. (19)) [56] showed the best fit with correlation coefficients very close to unity (R²=0.999) at all studied temperatures.

$$\frac{C_{inh}}{\theta} = \frac{1}{K_{ads}} + C \qquad (19)$$

where K_{ads} and θ refer to Langmuir adsorption equilibrium constant and surface coverage. The K_{ads}, which is obtained from the intercepts in Figure 6, is related to the standard Gibbs free energy of adsorption ΔG$^0_{ads}$ as follow [57]:

$$\Delta G^0_{ads} = -RT \ln (C_{solvant} \times K_{ads}) \qquad (20)$$

14

Where R, T, and $C_{solvant}$ denote the perfect gas constant (8.314 J K^{-1} mol^{-1}), the absolute temperature (K), and the concentration of water in solution (55.5 mol/l). Results are represented in Table 4, from which we can see that K_{ads} values decrease with the increase in temperatures. Obviously, this could be due to the desorption of HYD (*iso*) molecules at higher temperatures [29].

Table 4. Standard thermodynamic parameters of the adsorption of HYD (*iso*) in 1.0 M HCl solution.

Compound	T (K)	K_{ads} 10^{-3} (M^{-1})	R²	$-\Delta G^{\circ}_{ads}$ ($KJ\ mol^{-1}$)
HYD (*iso*)	298	56.80	0.999	37.07
	308	52.55	0.999	38.12
	318	45.17	0.999	38.96
	328	35.80	0.999	39.55

The values of ΔG^{0}_{ads} are tabulated in Table 4. The higher negative values of the standard free energy change of adsorption (ΔG^{0}_{ads}) approve that adsorption of inhibitor's molecules is proceeding spontaneously; they are ranging from -39.55 to -37.07 KJ mol^{-1}, which signifies that the adsorption of HYD (*iso*) occurs via a combination of physical and chemical processes [58,59].

3.5. Surface morphology

The surface morphology of CS samples after 2h immersion in blank and inhibited (5×10^{-3} M of HYD (*iso*)) solutions are displayed in Figure 7. Figure 7(a) displays a large damaged surface area in the absence of inhibitor; the corrosion products covered the whole surface due to the metal dissolution. However, the influence of the addition of HYD (*iso*) to the acid solution on the morphology of the steel surface is

evident, as observed in Figure 7(b). It is apparent **(***via* Figure 7(b)**)** that the dissolution of the metal substrate is remarkably decreased, and almost a smoother surface is achieved, suggesting that the studied compound is adsorbed on the metal surface and creating a protective film.

The presence of a protective film on the steel surface and its physical properties can be surveyed by contact angle measurements. The obtained results are displayed in Figure 8(a, b), from which we could see that the lowest contact angle (55.0°) was measured for the sample immersed in acidic solution. This could be due to the hydrophilic nature of the surface that makes the drop of water easily speared over the surface. In contrast, a significant change in the contact angle was observed in the presence of HYD (*iso*) (102.4°), confirming the presence of the hydrophobic film on the surface [60].

3.6. Quantum chemical calculation

3.6.1. Global reactivity descriptors

To establish a relationship between the inhibitor structure and its corrosion inhibition performance, and to unveil the inhibition mechanism, density functional theory (DFT) approach has been adopted. The optimized molecular structure, HOMOs, LUMOs, and molecular electrostatic potential maps were presented in Figure 9. It is obvious that the distribution of the HOMO density cover the entire molecular structure of HYD (*iso*). This could be attributed to the presence of a conjugation effect and a high electron density, which increases the electron-donating ability of the molecule, and thus an enhanced electron transfer interaction between inhibitor's reactive sites and

vacant orbitals of the metal [39]. On the other hand, the LUMO electron density is well distributed over the 2,4-dinitrophenyl cycle, which an indication of its high ability to receive electrons from the metal surface. Interestingly, the 2,4-dinitrophenyl moiety exhibits both characters, i.e., the ability to receive and dontae electrons, and therefore it is expected to play a crucial role in donor-acceptor interactions between inhibitor molecule and iron atoms. A similar conclusion could also be drawn from the the ESP map, where the red color, which stands for the negative region (nucleophilic attack) is located on the nitro groups ($-NO_2$), indicating its greatest ability to form a covalent bond with *d*-orbital of metal.

Some global reactivity descriptors calculated in the aqueous phase are listed in Table 5. It is well-known that a higher E_{HOMO} values reveal a high electron-donating ability while a lower value of E_{LUMO} signifies the propensity of a molecule to accept electrons. Moreover, the energy gap ΔE is another index of reactivity of molecules. A lower value of ΔE indicates that an inhibitor molecule is more polarizable and could strongly interact wih a metal surface [61]. While it is not possible to discuss these parameters without comparing them with those of a similar compound, it is important to note that energy gap of the present molecule is very low, compared to many reported corrosion inhibitors [40,41,62]. Yet again, this observation confirms our finding that the investigated hydrazone derivative has outstanding corrosion inhibition effects. The obtained ΔN value is positive, suggesting a high electron sharing tendency between inhibitor's molecule and the metal surface [62].

Table 5. Calculated quantum chemical indices of the studied compound.

Descriptors	E_{HOMO} (eV)	E_{LUMO} (eV)	ΔE (eV)	ΔN
HYD (*iso*)	-5.355	-3.725	1.630	0.086

3.6.2. Active sites

The active sites responsible for donor-acceptor (D-A) type interactions between inhibitor molecule and iron surface can be determined more precisely from neutral atomic charge distribution and Fukui indices [63]. The Mulliken charges and Fukui indices of HYD (*iso*) are displayed in Figure S3. It is reported that a higher negative charge of heteroatom means a high electronic density, and indicates a high tendency for participation in the D-A types of interaction [64]. The analysis of Mulliken results represented in Figure S3 indicates that a high negative Mulliken atomic charge occur on N8, N9, O27, O28, O29, O30 atoms, and some carbon atoms as well. They are expected to be involved in interactions with the metal surface and are the most susceptible reactive sites for adsorption [41]. The widespread distribution of reactive sites is likely one of reasons why tested compound has a potent corrosion inhibition performance.

The Fukui indices are significant for analyzing the local reactive sites responsible for the nucleophilic and electrophilic behavior of an inhibitor. Based on literature, atoms with high values of f_k^+ indicate that these sites have a nucleophilic attack character, whereas those having higher values of f_k^- are prone to electrophilic attack [20]. From the calculated Fukui indices, the most preferable sites for the electrophilic attack are located in the N (8), N (9), C (11), O (27), O (28), O (29) and O (30) atoms with the most positive part of f_k^-, whereas the C (14), N (26), O (27), O (28), O (29) and O (30), are the most reactive sites for the nucleophilic attack. Both Fukui indices and Mullikan distribution results are in good agreement with the frontier orbital distribution of inhibitor.

From the above analysis, we could conclude that the high inhibitory power of HYD (*iso*) is a result of its widespread active sites, which play the key role in D-A interactions with the metal surface.

3.7. Molecular dynamics simulation

To assess the adsorption of the inhibitor molecule on metal surfaces in a mimic condition, MD simulations were performed. Figure 10(a)-(b) displays top and side views of the optimized adsorption configuration of HYD (*iso*) on the iron surface (in its most stable plane, i.e., (110)). A close examination of the figure revealed that the adsorption of the studied inhibitor on the iron surface is almost parallel, indicating a maximum coverage, which in turn leads to a high interaction with the iron surface. The obtained $E_{\text{interaction}}$ value of HYD (*iso*) on Fe (110) surface is -2402.94 Kcal/mol. This larger negative value suggests that the adsorption of the hydrazone molecule on the iron surface is spontaneous and strong. Radial distribution function (RDF) g(r) (or pair correlation function) is a mathematical tool that describes the shape and positions of a particle with respect to one another. It is defined as follows [65]:

$$g_{AB}(r) = \frac{1}{<\rho_B>} \times \frac{1}{N_A} \sum_{i \in A}^{N_A} \sum_{j \in B}^{N_A} \frac{\delta(r_{ij}-r)}{4\pi r^2} \qquad (21)$$

where $<\rho_B>$ represents the particle density of B averaged over all shells around particle A.

In general, chemical interactions showing a peak at a position between 1 and 3.5 Å, while peaks located at more than 3.5 Å characterize physical interactions [31]. In

19

present RDF results (*via* Figure 10(c)), the first prominent peak is located at 3.01 Å, which suggests a chemical bonds formation between the hydrazone molecule and iron atoms. Moreover, several other peaks located outside 3.5 Å may be attributed to physical interactions. Together, these results further support those from experimental and quantum chemical investigations.

3.8. Protection mechanism and comparison with other hydrazones

Generally, the mechanism of action of corrosion inhibitor on metal surface in acid medium is supposed to be influenced by the chemical structure of the inhibitor molecules, the nature and charge of the metal. Through the above results, the adsorption of HYD (*iso*) on CS surface can be explained as follows:

- Corrosion inhibition experiments were carried out in HCl medium, which leads to a positive charge of the metal surface [66]. In addition, the tested inhibitors are expected to be protonated. In this form, the positive charge of the metal will favor the adsorption of chlorides (Cl$^-$) on its surface, creating a bridge between charged metallic surface and protonated inhibitor molecules, and thus results in increases in the attractive forces between them. This suggestion is supported by XPS results, which indicated the presence of a charged nitrogen atom. At this stage, corrosion protection is driven primarily by physisorption, therefore, blocking reaction sites of the mild steel [40].

- As demonstrated in the results described above, the corrosion process could be also blocked by chemisorption. The presence of electron-rich aromatic rings and heteroatoms is expected to increase the transfer of loosely bound electrons from molecules to electron-deficient iron orbitals. Within this

mechanism, the presence of two aromatic rings enables the inhibitor's molecule to donate π-electrons to unfilled iron orbitals [41].

- Along with these interactions, it should also be emphasized that the high molecular weight and the large size of the hydrazone derivative can also be considered as another factor that may influence its adsorption on the metal surface. Figure 11 represents all possible interactions between the hydrazone derivative and the iron surface.

In several recent papers, one can find several hydrazone derivatives tested for corrosion inhibition of different metal and alloys. This family of inhibitors has demonstrated good ability to inhibit metal corrosion. A comparison with other hydrazone derivatives in acid media is given in Table 6, and HYD (iso) exhibited better corrosion inhibition behavior.

Table 6. Comparison of the inhibition efficiency of HYD (iso) with that of some hydrazone derivatives previously published.

Inhibitor/ Concentration	Metal/ Medium	Inhibition efficiency (%)	Reference
HZD[2]	Mild steel/1 M HCl	94	[67]
HZD[3]	Mild steel/1 M HCl	92	[67]
HZD[4]	Mild steel/1 M HCl	86	[67]
2-ABNH	Mild steel/1 M HCl	95	[68]
HZD-1	Mild steel/1 M HCl	95	[20]
HZD-2	Mild steel/1 M HCl	90	[20]
HZD-3	Mild steel/1 M HCl	84	[20]
TH-1	Mild steel/0.5 M HCl	86	[21]

TH-2	Mild steel/0.5 M HCl	89	[21]
TH-3	Mild steel/0.5 M HCl	90	[21]
HYD (*iso*)	Mild steel/1 M HCl	97	This work

4. Conclusion

In the present study, a new synthesized hydrazone derivative was evaluated as corrosion inhibitor for the carbon steel/1.0 M HCl system. The study revealed that HYD (*iso*) acted as a good corrosion inhibitor and its effectiveness increases by concentration. The adsorption mode of HYD (*iso*) on the CS surface obeys to Langmuir adsorption isotherm. The spontaneity of adsorption was justified by negative values of ΔG^0_{ads}, and their value reveals a combination of physical and chemical interactions. Electrochemical results indicated that the hydrazone derivative acted as a mixed-type inhibitor, also, the increment in the values of R_p with increasing concentration showed the effective adsorption of inhibitor on the surface. SEM, contact angle and XPS analysis explained well enough why the investigated compound is an efficient corrosion inhibitor and how it exerts its corrosion inhibition effect. Computational calculations supported experimental findings by providing useful theoretical insights. The results indicated that the presence of nitro groups makes the tested compound an excellent corrosion inhibitor, thereby providing a highest inhibition efficiency compared to previously studied hydrazone derivatives. Thus, this study could be a target for future research efforts in the corrosion inhibition field.

"Declaration of competing interest

The authors declare that they have no known competing financial interests or personal relationships that could have appeared to influence the work reported in this paper."

References

[1] Z. Sanaei, G. Bahlakeh, B. Ramezanzadeh, M. Ramezanzadeh, Application of green molecules from Chicory aqueous extract for steel corrosion mitigation against chloride ions attack; the experimental examinations and electronic/atomic level computational studies, J. Mol. Liq. 290 (2019) 111176. https://doi.org/10.1016/j.molliq.2019.111176.

[2] A. Dehghani, G. Bahlakeh, B. Ramezanzadeh, M. Ramezanzadeh, A combined experimental and theoretical study of green corrosion inhibition of mild steel in HCl solution by aqueous Citrullus lanatus fruit (CLF) extract, J. Mol. Liq. 279 (2019) 603–624. https://doi.org/10.1016/j.molliq.2019.02.010.

[3] R.K. Gupta, M. Malviya, C. Verma, M. Quraishi, Aminoazobenzene and diaminoazobenzene functionalized graphene oxides as novel class of corrosion inhibitors for mild steel: experimental and DFT studies, Mater. Chem. Phys. 198 (2017) 360–373.

[4] C. Verma, M. Quraishi, E.E. Ebenso, I. Bahadur, A green and sustainable approach for mild steel acidic corrosion inhibition using leaves extract: experimental and DFT studies, J. Bio- Tribo-Corros. 4 (2018) 33.

[5] S.K. Ahmed, W.B. Ali, A.A. Khadom, Synthesis and investigations of heterocyclic compounds as corrosion inhibitors for mild steel in hydrochloric acid, Int. J. Ind. Chem. 10 (2019) 159–173.

[6] R.T. Loto, C.A. Loto, Inhibition studies of the synergistic effect of chemical compounds on 3CR12 ferritic steel corrosion in acid solutions, Chem. Data Collect. 22 (2019) 100255.

[7] Y. Qiang, S. Zhang, S. Xu, W. Li, Experimental and theoretical studies on the corrosion inhibition of copper by two indazole derivatives in 3.0% NaCl solution, J. Colloid Interface Sci. 472 (2016) 52–59.

[8] S. Ralkhal, T. Shahrabi, B. Ramezanzadeh, Synthesis and construction of a highly potent hybrid organic/inorganic anti-corrosive pigment for effective corrosion control of mild steel in simulated seawater, Constr. Build. Mater. 222 (2019) 400–413.

[9] C. Zhang, J. Zhao, Synergistic inhibition effects of octadecylamine and tetradecyl trimethyl ammonium bromide on carbon steel corrosion in the H2S and CO2 brine solution, Corros. Sci. 126 (2017) 247–254.

[10] B.J. Usman, S.A. Umoren, Z.M. Gasem, Inhibition of API 5L X60 steel corrosion in CO2-saturated 3.5% NaCl solution by tannic acid and synergistic effect of KI additive, J. Mol. Liq. 237 (2017) 146–156.

[11] K. Abderrahim, I. Selatnia, A. Sid, P. Mosset, 1, 2-bis (4-chlorobenzylidene) Azine as new and effective corrosion inhibitor for copper in 0.1 N HCl: a combined experimental and theoretical approach, Chem. Phys. Lett. 707 (2018) 117–128.

[12] K. Khaled, Corrosion control of copper in nitric acid solutions using some amino acids–A combined experimental and theoretical study, Corros. Sci. 52 (2010) 3225–3234.

[13] H.M.A. El-Lateef, Experimental and computational investigation on the corrosion inhibition characteristics of mild steel by some novel synthesized imines in hydrochloric acid solutions, Corros. Sci. 92 (2015) 104–117.

[14] H.M.A. El-Lateef, A.M. Abu-Dief, L.H. Abdel-Rahman, E.C. Sañudo, N. Aliaga-Alcalde, Electrochemical and theoretical quantum approaches on the inhibition of C1018 carbon steel corrosion in acidic medium containing chloride using some newly synthesized phenolic Schiff bases compounds, J. Electroanal. Chem. 743 (2015) 120–133.

[15] G. Sığırcık, T. Tüken, M. Erbil, Inhibition efficiency of aminobenzonitrile compounds on steel surface, Appl. Surf. Sci. 324 (2015) 232–239.

[16] A. Fouda, S. Abd El-Maksoud, A. El-Hossiany, A. Ibrahim, Evolution of the corrosion-inhibiting efficiency of novel hydrazine derivatives against corrosion of stainless steel 201 in acidic medium, Int J Electrochem Sci. 14 (2019) 2187–2207.

[17] S. Rollas, S.G. Küçükgüzel, Biological activities of hydrazone derivatives, Molecules. 12 (2007) 1910–1939.

[18] H. Lgaz, A. Chaouiki, M.R. Albayati, R. Salghi, Y. El Aoufir, I.H. Ali, M.I. Khan, S.K. Mohamed, I.-M. Chung, Synthesis and evaluation of some new hydrazones as corrosion inhibitors for mild steel in acidic media, Res. Chem. Intermed. 45 (2019) 2269–2286.

[19] N. Chafai, S. Chafaa, K. Benbouguerra, A. Hellal, M. Mehri, Synthesis, spectral analysis, anti-corrosive activity and theoretical study of an aromatic hydrazone derivative, J. Mol. Struct. 1181 (2019) 83–92.

[20] H. Lgaz, I.-M. Chung, M.R. Albayati, A. Chaouiki, R. Salghi, S.K. Mohamed, Improved corrosion resistance of mild steel in acidic solution by hydrazone derivatives: an experimental and computational study, Arab. J. Chem. 13 (2020) 2934–2954.

[21] T.K. Chaitra, K.N. Mohana, D.M. Gurudatt, H.C. Tandon, Inhibition activity of new thiazole hydrazones towards mild steel corrosion in acid media by thermodynamic, electrochemical and quantum chemical methods, J. Taiwan Inst. Chem. Eng. 67 (2016) 521–531.

[22] L. Guo, I.B. Obot, X. Zheng, X. Shen, Y. Qiang, S. Kaya, C. Kaya, Theoretical insight into an empirical rule about organic corrosion inhibitors containing nitrogen, oxygen, and sulfur atoms, Appl. Surf. Sci. 406 (2017) 301–306. https://doi.org/10.1016/j.apsusc.2017.02.134.

[23] L. Guo, C. Qi, X. Zheng, R. Zhang, X. Shen, S. Kaya, Toward understanding the adsorption mechanism of large size organic corrosion inhibitors on an Fe(110) surface using the DFTB method, RSC Adv. 7 (2017) 29042–29050. https://doi.org/10.1039/C7RA04120A.

[24] H. Lgaz, R. Salghi, I.H. Ali, Corrosion Inhibition Behavior of 9-Hydroxyrisperidone as a Green Corrosion Inhibitor for Mild Steel in Hydrochloric Acid: Electrochemical, DFT and MD Simulations Studies, Int. J. Electrochem. Sci. 13 (2018) 250–264. https://doi.org/10.2964/2018.01.26.

[25] S. Akbarzadeh, B. Ramezanzadeh, G. Bahlakeh, M. Ramezanzadeh, Molecular/electronic/atomic-level simulation and experimental exploration of the corrosion inhibiting molecules attraction at the steel/chloride-containing solution

interface, J. Mol. Liq. 296 (2019) 111809. https://doi.org/10.1016/j.molliq.2019.111809.

[26] G. Bahlakeh, A. Dehghani, B. Ramezanzadeh, M. Ramezanzadeh, Highly effective mild steel corrosion inhibition in 1 M HCl solution by novel green aqueous Mustard seed extract: Experimental, electronic-scale DFT and atomic-scale MC/MD explorations, J. Mol. Liq. 293 (2019) 111559. https://doi.org/10.1016/j.molliq.2019.111559.

[27] P. American Society for Testing and Materials (Filadelfia, ASTM G1-03: Standard Practice for Preparing, Cleaning, and Evaluating Corrosion Test Specimens, in: ASTM, 2004.

[28] G. ASTM, 31-72, Standard Practice for Laboratory Immersion Corrosion Testing of Metals; ASTM: Philadelphia, PA, 1990, There No Corresp. Rec. This Ref. Sch. (n.d.).

[29] N. Djeddi, M. Benahmed, S. Akkal, H. Laouer, E. Makhloufi, N. Gherraf, Study on methylene dichloride and butanolic extracts of Reutera lutea (Desf.) Maire (Apiaceae) as effective corrosion inhibitions for carbon steel in HCl solution, Res. Chem. Intermed. 41 (2015) 4595–4616.

[30] K. Orubite, N. Oforka, Inhibition of the corrosion of mild steel in hydrochloric acid solutions by the extracts of leaves of Nypa fruticans Wurmb, Mater. Lett. 58 (2004) 1768–1772.

[31] H. Lgaz, I.-M. Chung, R. Salghi, I.H. Ali, A. Chaouiki, Y. El Aoufir, M.I. Khan, On the understanding of the adsorption of Fenugreek gum on mild steel in an acidic medium: Insights from experimental and computational studies, Appl. Surf. Sci. 463 (2019) 647–658. https://doi.org/10.1016/j.apsusc.2018.09.001.

[32] M. Benahmed, I. Selatnia, A. Achouri, H. Laouer, N. Gherraf, S. Akkal, Steel corrosion inhibition by Bupleurum lancifolium (Apiaceae) extract in acid solution, Trans. Indian Inst. Met. 68 (2015) 393–401.

[33] S. Boudiba, K. Hanini, I. Selatnia, A. Saouane, S. Hioun, M. Benahmed, Experimental, theoretical and mathematical studies of Echium italicum L. extract as a corrosion inhibitor for carbon steel in acidic medium, Mater. Res. Express. 6 (2019) 086546.

[34] J.P. Perdew, K. Burke, M. Ernzerhof, Generalized gradient approximation made simple, Phys. Rev. Lett. 77 (1996) 3865.

[35] A. Klamt, G. Schüürmann, COSMO: a new approach to dielectric screening in solvents with explicit expressions for the screening energy and its gradient, J. Chem. Soc. Perkin Trans. 2. (1993) 799–805.

[36] R.L. Akkermans, N.A. Spenley, S.H. Robertson, Monte Carlo methods in materials studio, Mol. Simul. 39 (2013) 1153–1164.

[37] L. Guo, S. Kaya, I.B. Obot, X. Zheng, Y. Qiang, Toward understanding the anticorrosive mechanism of some thiourea derivatives for carbon steel corrosion: A combined DFT and molecular dynamics investigation, J. Colloid Interface Sci. 506 (2017) 478–485. https://doi.org/10.1016/j.jcis.2017.07.082.

[38] L. Guo, Z.S. Safi, S. Kaya, W. Shi, B. Tüzün, N. Altunay, C. Kaya, Anticorrosive Effects of Some Thiophene Derivatives Against the Corrosion of Iron: A Computational Study, Front. Chem. 6 (2018). https://doi.org/10.3389/fchem.2018.00155.

[39] I. Selatnia, A. Sid, M. Benahmed, O. Dammene debbih, T. Ozturk, N. Gherraf, Synthesis and Characterization of a Bis-Pyrazoline Derivative as Corrosion Inhibitor for A283 Carbon Steel in 1M HCl: Electrochemical, Surface, DFT and

MD Simulation Studies, Prot. Met. Phys. Chem. Surf. 54 (2018) 1182–1193. https://doi.org/10.1134/S2070205118060229.

[40] Y. El Aoufir, R. Aslam, F. Lazrak, R. Marzouki, S. Kaya, S. Skal, A. Ghanimi, I.H. Ali, A. Guenbour, H. Lgaz, I.-M. Chung, The effect of the alkyl chain length on corrosion inhibition performances of 1,2,4-triazole-based compounds for mild steel in 1.0 M HCl: Insights from experimental and theoretical studies, J. Mol. Liq. 303 (2020) 112631. https://doi.org/10.1016/j.molliq.2020.112631.

[41] H. Lgaz, S.Kr. Saha, A. Chaouiki, K.S. Bhat, R. Salghi, Shubhalaxmi, P. Banerjee, I.H. Ali, M.I. Khan, I.-M. Chung, Exploring the potential role of pyrazoline derivatives in corrosion inhibition of mild steel in hydrochloric acid solution: Insights from experimental and computational studies, Constr. Build. Mater. 233 (2020) 117320. https://doi.org/10.1016/j.conbuildmat.2019.117320.

[42] A. Dehghani, A.H. Mostafatabar, G. Bahlakeh, B. Ramezanzadeh, M. Ramezanzadeh, Detailed-level computer modeling explorations complemented with comprehensive experimental studies of Quercetin as a highly effective inhibitor for acid-induced steel corrosion, J. Mol. Liq. 309 (2020) 113035. https://doi.org/10.1016/j.molliq.2020.113035.

[43] H. Li, S. Zhang, B. Tan, Y. Qiang, W. Li, S. Chen, L. Guo, Investigation of Losartan Potassium as an eco-friendly corrosion inhibitor for copper in 0.5 M H2SO4, J. Mol. Liq. 305 (2020) 112789. https://doi.org/10.1016/j.molliq.2020.112789.

[44] B. Chugh, A.K. Singh, A. Chaouiki, R. Salghi, S. Thakur, B. Pani, A comprehensive study about anti-corrosion behaviour of pyrazine carbohydrazide: Gravimetric, electrochemical, surface and theoretical study, J. Mol. Liq. 299 (2020) 112160. https://doi.org/10.1016/j.molliq.2019.112160.

[45] M. Yadav, T. K. Sarkar, I. B. Obot, Carbohydrate compounds as green corrosion inhibitors: electrochemical, XPS, DFT and molecular dynamics simulation studies, RSC Adv. 6 (2016) 110053–110069. https://doi.org/10.1039/C6RA24026G.

[46] A. Singh, K.R. Ansari, A. Kumar, W. Liu, C. Songsong, Y. Lin, Electrochemical, surface and quantum chemical studies of novel imidazole derivatives as corrosion inhibitors for J55 steel in sweet corrosive environment, J. Alloys Compd. 712 (2017) 121–133. https://doi.org/10.1016/j.jallcom.2017.04.072.

[47] V. Kumar K, A.R.B. V, Chemically modified biopolymer as an eco-friendly corrosion inhibitor for mild steel in a neutral chloride environment, New J. Chem. 41 (2017) 6278–6289. https://doi.org/10.1039/C7NJ00553A.

[48] D.S. Kharitonov, J. Sommertune, C. Örnek, J. Ryl, I.I. Kurilo, P.M. Claesson, J. Pan, Corrosion inhibition of aluminium alloy AA6063-T5 by vanadates: Local surface chemical events elucidated by confocal Raman micro-spectroscopy, Corros. Sci. 148 (2019) 237–250. https://doi.org/10.1016/j.corsci.2018.12.011.

[49] C. Ruttanapun, Effects of Pd substitution on the thermoelectric and electronic properties of delafossite Cu1−xPdxFeO2 (x=0.01, 0.03 and 0.05), J. Solid State Chem. 215 (2014) 43–49. https://doi.org/10.1016/j.jssc.2014.03.027.

[50] H. Kanatani, H. Kume, T. Matsui, Magnetic properties of SrTiO3-buffered Ba(Fe0.2Zr0.8)O3−δ films on Si(001) substrates, J. Appl. Phys. 105 (2009) 07D907. https://doi.org/10.1063/1.3059407.

[51] A. Dehghani, G. Bahlakeh, B. Ramezanzadeh, M. Ramezanzadeh, Integrated modeling and electrochemical study of Myrobalan extract for mild steel corrosion retardation in acidizing media, J. Mol. Liq. 298 (2020) 112046. https://doi.org/10.1016/j.molliq.2019.112046.

[52] K. Hanini, B. Merzoug, S. Boudiba, I. Selatnia, H. Laouer, S. Akkal, Influence of different polyphenol extracts of Taxus baccata on the corrosion process and their effect as additives in electrodeposition, Sustain. Chem. Pharm. 14 (2019) 100189. https://doi.org/10.1016/j.scp.2019.100189.

[53] M. Benahmed, I. Selatnia, N. Djeddi, S. Akkal, H. Laouer, Adsorption and Corrosion Inhibition Properties of Butanolic Extract of Elaeoselinum thapsioides and Its Synergistic Effect with Reutera lutea (Desf.) Maires (Apiaceae) on A283 carbon Steel in Hydrochloric Acid Solution, Chem. Afr. 3 (2020) 251–261. https://doi.org/10.1007/s42250-019-00093-8.

[54] M.A. Hegazy, M. Abdallah, M.K. Awad, M. Rezk, Three novel di-quaternary ammonium salts as corrosion inhibitors for API X65 steel pipeline in acidic solution. Part I: Experimental results, Corros. Sci. 81 (2014) 54–64. https://doi.org/10.1016/j.corsci.2013.12.010.

[55] J. Zhang, X.L. Gong, H.H. Yu, M. Du, The inhibition mechanism of imidazoline phosphate inhibitor for Q235 steel in hydrochloric acid medium, Corros. Sci. 53 (2011) 3324–3330. https://doi.org/10.1016/j.corsci.2011.06.008.

[56] A. Chaouiki, H. Lgaz, R. Salghi, M. Chafiq, H. Oudda, Shubhalaxmi, K.S. Bhat, I. Cretescu, I.H. Ali, R. Marzouki, I.-M. Chung, Assessing the impact of electron-donating-substituted chalcones on inhibition of mild steel corrosion in HCl solution: Experimental results and molecular-level insights, Colloids Surf. Physicochem. Eng. Asp. 588 (2020) 124366. https://doi.org/10.1016/j.colsurfa.2019.124366.

[57] A. El Bribri, M. Tabyaoui, B. Tabyaoui, H. El Attari, F. Bentiss, The use of Euphorbia falcata extract as eco-friendly corrosion inhibitor of carbon steel in hydrochloric acid solution, Mater. Chem. Phys. 141 (2013) 240–247. https://doi.org/10.1016/j.matchemphys.2013.05.006.

[58] C. Verma, E.E. Ebenso, I. Bahadur, I.B. Obot, M.A. Quraishi, 5-(Phenylthio)-3H-pyrrole-4-carbonitriles as effective corrosion inhibitors for mild steel in 1M HCl: Experimental and theoretical investigation, J. Mol. Liq. 212 (2015) 209–218. https://doi.org/10.1016/j.molliq.2015.09.009.

[59] S.C. Nwanonenyi, H.C. Obasi, I.O. Eze, Hydroxypropyl Cellulose as an Efficient Corrosion Inhibitor for Aluminium in Acidic Environments: Experimental and Theoretical Approach, Chem. Afr. 2 (2019) 471–482. https://doi.org/10.1007/s42250-019-00062-1.

[60] A. Singh, K.R. Ansari, D.S. Chauhan, M.A. Quraishi, H. Lgaz, I.-M. Chung, Comprehensive investigation of steel corrosion inhibition at macro/micro level by ecofriendly green corrosion inhibitor in 15% HCl medium, J. Colloid Interface Sci. 560 (2020) 225–236. https://doi.org/10.1016/j.jcis.2019.10.040.

[61] B.T. Ogunyemi, D.F. Latona, I.A. Adejoro, Molecular modeling and quantitative structure–property relationships (QSPRs) of purine derivatives as corrosion inhibitor in acid medium, Sci. Afr. 8 (2020) e00336. https://doi.org/10.1016/j.sciaf.2020.e00336.

[62] H. Lgaz, R. Salghi, S. Masroor, S.-H. Kim, C. Kwon, S.Y. Kim, Y.-J. Yang, I.-M. Chung, Assessing corrosion inhibition characteristics of hydrazone derivatives on mild steel in HCl: Insights from electronic-scale DFT and atomic-scale molecular dynamics, J. Mol. Liq. 308 (2020) 112998. https://doi.org/10.1016/j.molliq.2020.112998.

[63] H. Mi, G. Xiao, X. Chen, Theoretical evaluation of corrosion inhibition performance of three antipyrine compounds, Comput. Theor. Chem. 1072 (2015) 7–14.

[64] S.Kr. Saha, M. Murmu, N.C. Murmu, I.B. Obot, P. Banerjee, Molecular level insights for the corrosion inhibition effectiveness of three amine derivatives on the carbon steel surface in the adverse medium: A combined density functional theory and molecular dynamics simulation study, Surf. Interfaces. 10 (2018) 65–73. https://doi.org/10.1016/j.surfin.2017.11.007.

[65] J.-P. Hansen, I.R. McDonald, Theory of Simple Liquids: with Applications to Soft Matter, Academic Press, 2013.

[66] R. Solmaz, Investigation of adsorption and corrosion inhibition of mild steel in hydrochloric acid solution by 5-(4-Dimethylaminobenzylidene)rhodanine, Corros. Sci. 79 (2014) 169–176. https://doi.org/10.1016/j.corsci.2013.11.001.

[67] H. Lgaz, A. Chaouiki, M.R. Albayati, R. Salghi, Y. El Aoufir, I.H. Ali, M.I. Khan, S.K. Mohamed, I.-M. Chung, Synthesis and evaluation of some new hydrazones as corrosion inhibitors for mild steel in acidic media, Res. Chem. Intermed. 45 (2019) 2269–2286.

[68] D.K. Singh, S. Kumar, G. Udayabhanu, R.P. John, 4 (N, N-dimethylamino) benzaldehyde nicotinic hydrazone as corrosion inhibitor for mild steel in 1 M HCl solution: An experimental and theoretical study, J. Mol. Liq. 216 (2016) 738–746.

Figure captions:

Fig. 1. Variation of corrosion rate (a) and inhibition efficiency (b) as a function of concentration after 2 hours of immersion time in 1.0 M HCl at different temperatures.

Fig. 2. XPS survey spectrum of HYD (*iso*) treated-carbon steel in 1.0 M HCl.

Fig. 3. XPS spectra of CS specimens in the presence of 5×10^{-3} M of HYD (iso): (a) C 1s, (b) O 1s, (c) N 1s, and (d) Fe $2p_{3/2}$.

Fig 4. EIS results: (a) Nyquist; (b) and (c) Bode and phase angle plots for CS in 1.0 M HCl with and without various concentrations of HYD (*iso*) at 298 K; (d) Equivalent circuit used to fit the EIS data.

Fig 5. Potentiodynamic polarization curves for CS steel obtain in 1.0 M HCl in the absence and presence of different concentrations of HYD (*iso*).

Fig. 6. Langmuir isotherm adsorption of HYD (*iso)* on the CS in 1.0 M HCl at different temperatures.

Fig. 7. SEM micrograph of CS surface (a) in the absence of inhibitor and (b) in the presence of 5×10^{-3} M of inhibitor.

Fig. 8. Water contact angle results for the unprotected (a) and protected sample (b).

Fig. 9. The optimized structures, frontier orbital density distributions, and electrostatic potential (ESP) map of HYD (*iso*) molecule in the aqueous phase.

Fig. 10. Equilibrium adsorption configuration of the HYD (*iso*) on the Fe (110) obtained from MD simulations. (a) Top view, (b) Side view and (c) RDF curve for the HYD *(iso)* on Fe (110) surface.

Fig. 11. Possible interactions between inhibitor molecule and carbon steel surface.
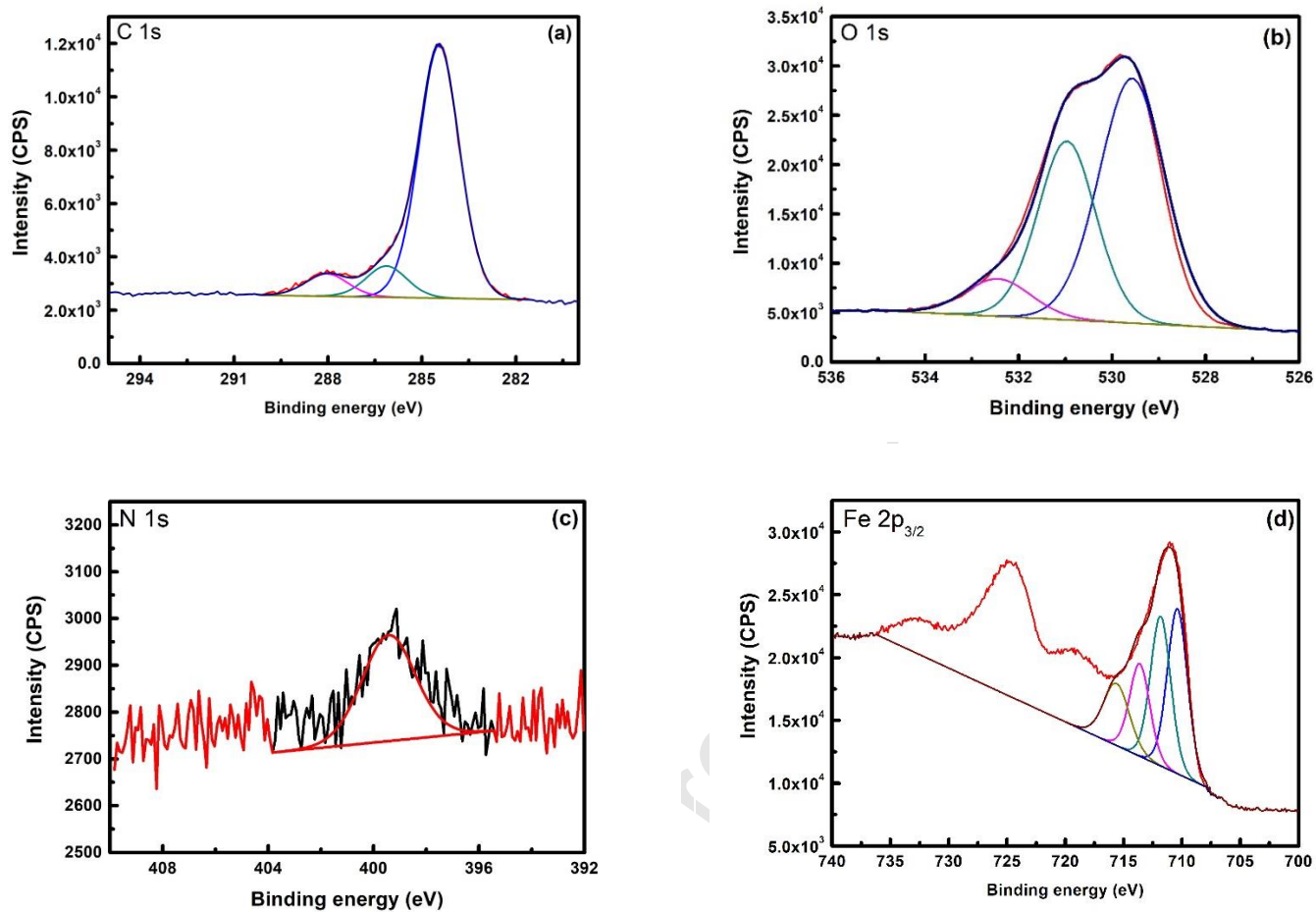
Figure 1.
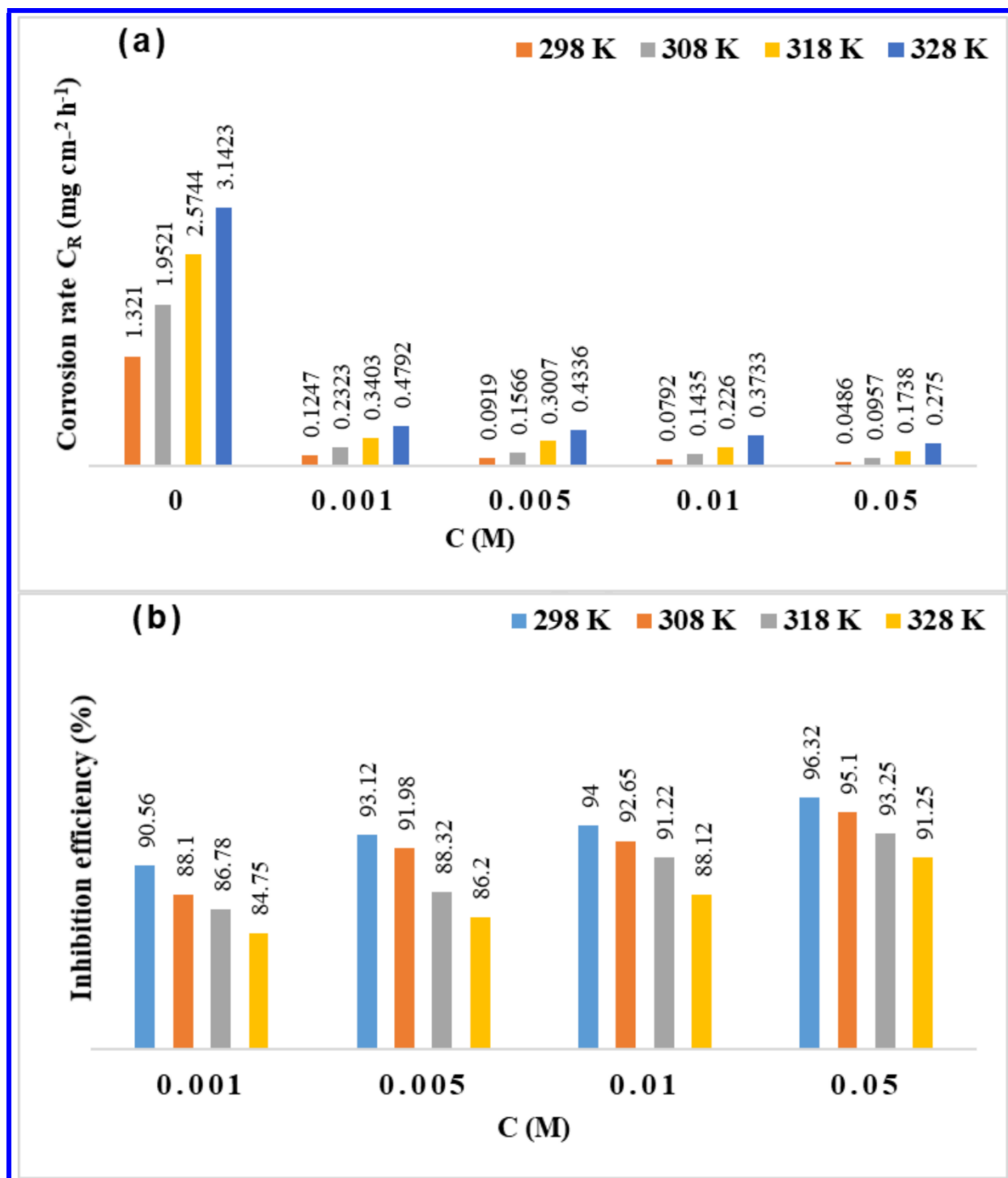
Figure 2.
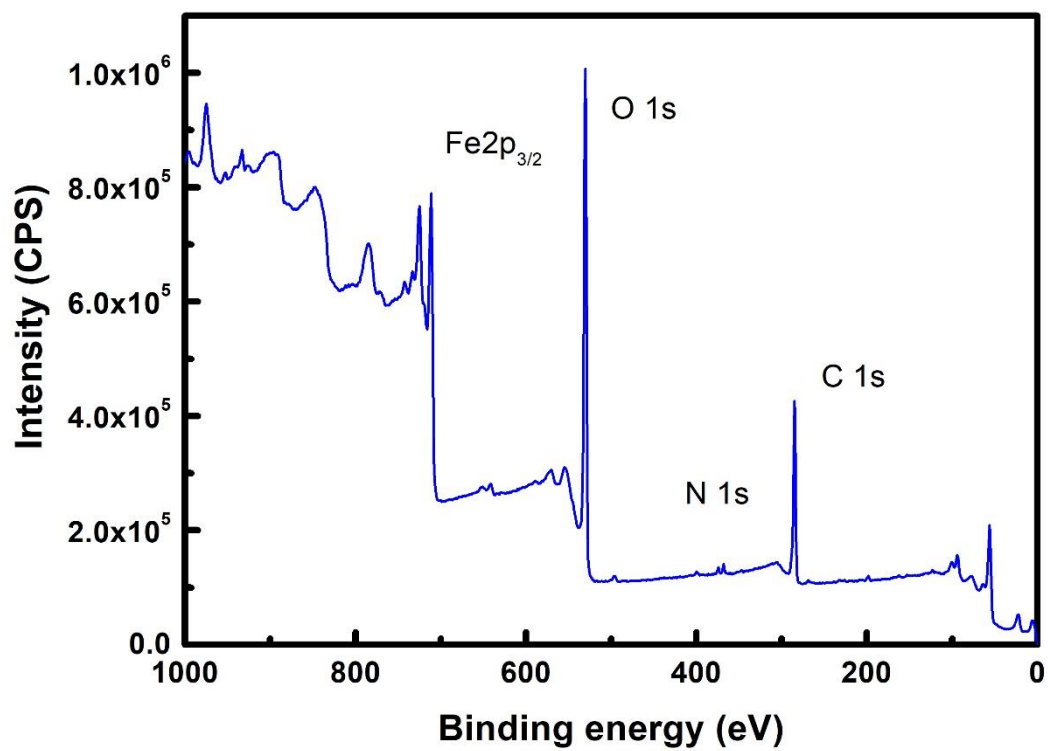
Figure 3.

Figure 4.
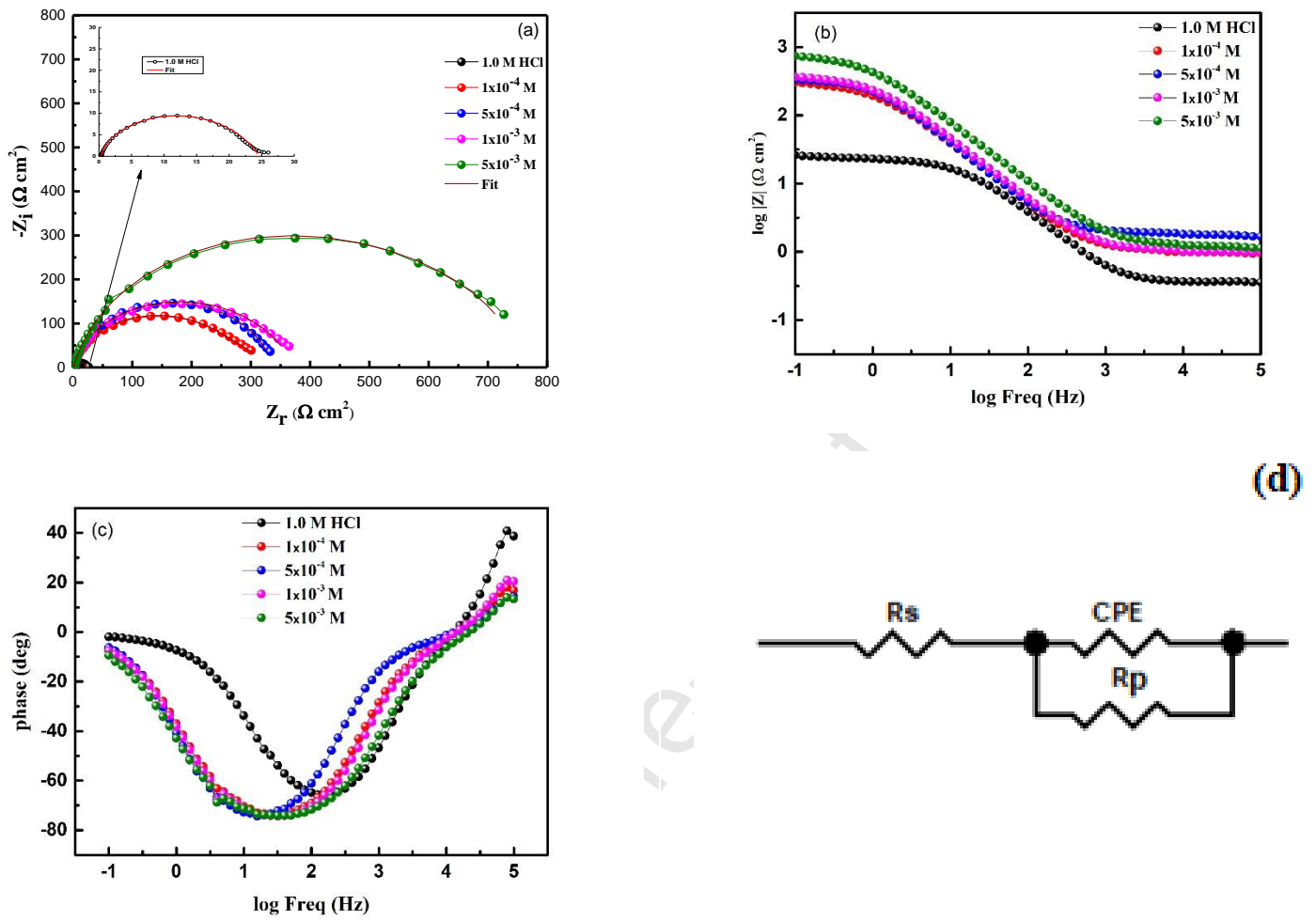
Figure 5.
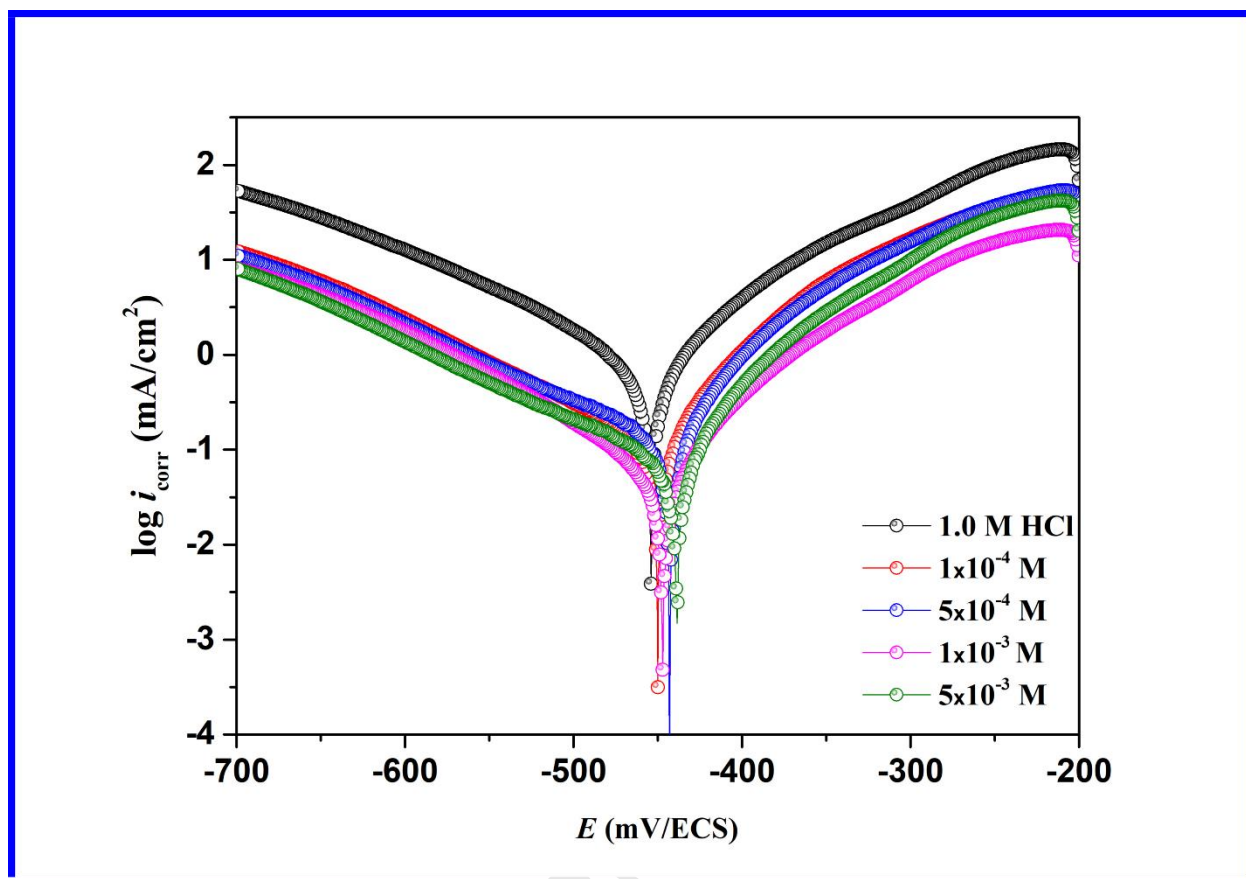
Figure 6.
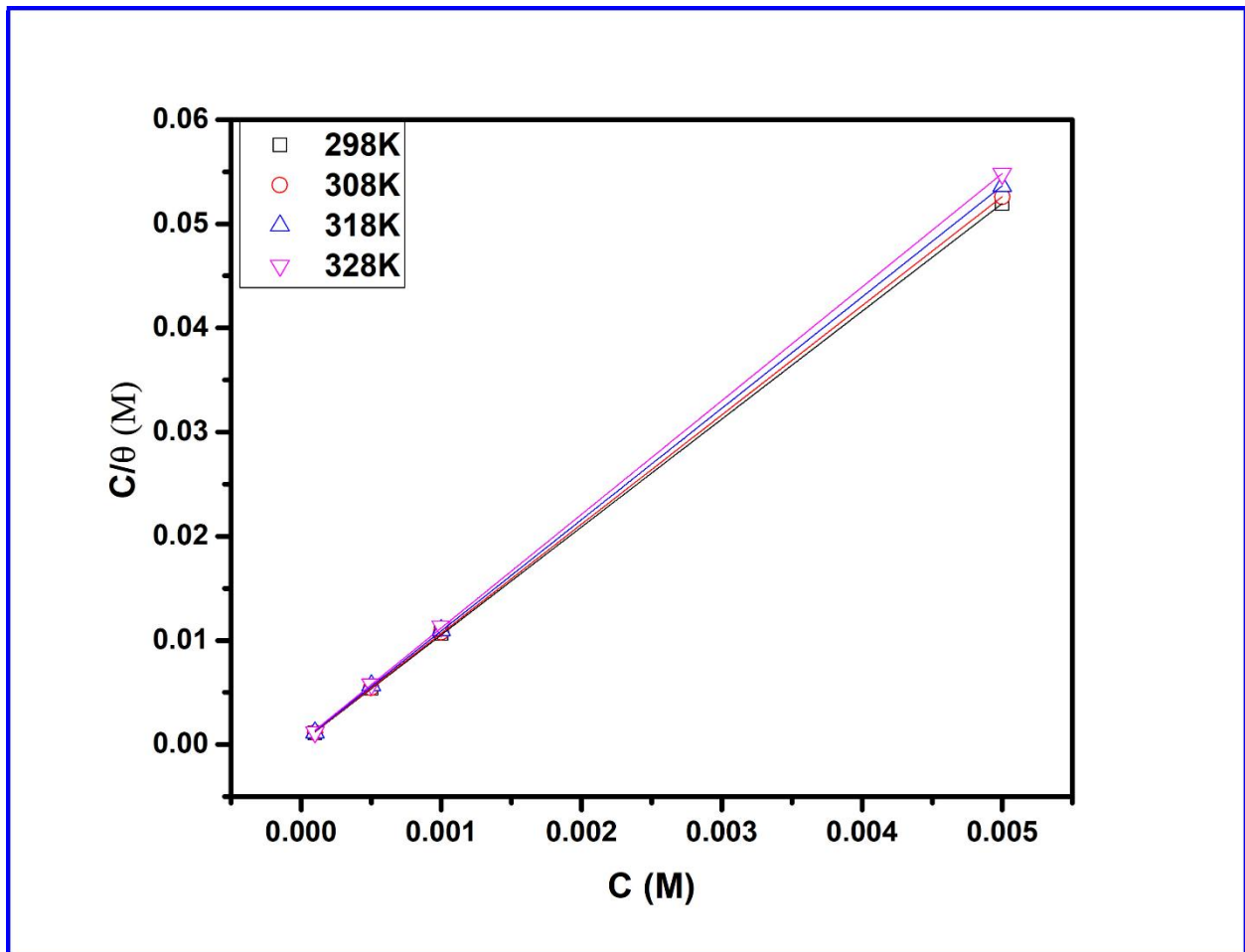
Figure 7.

Figure 8.

Figure 9.

Optimized molecular structure
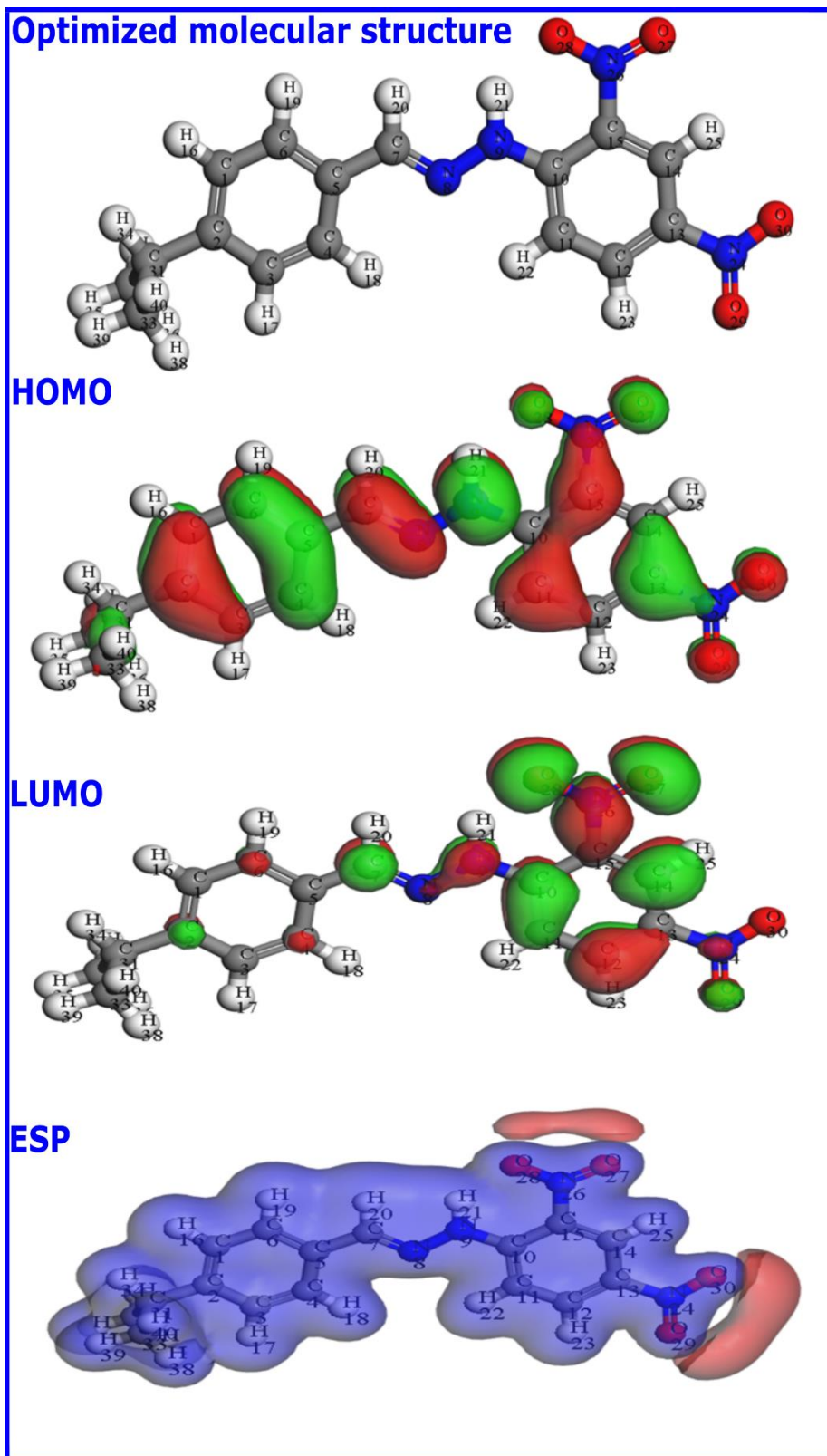
HOMO
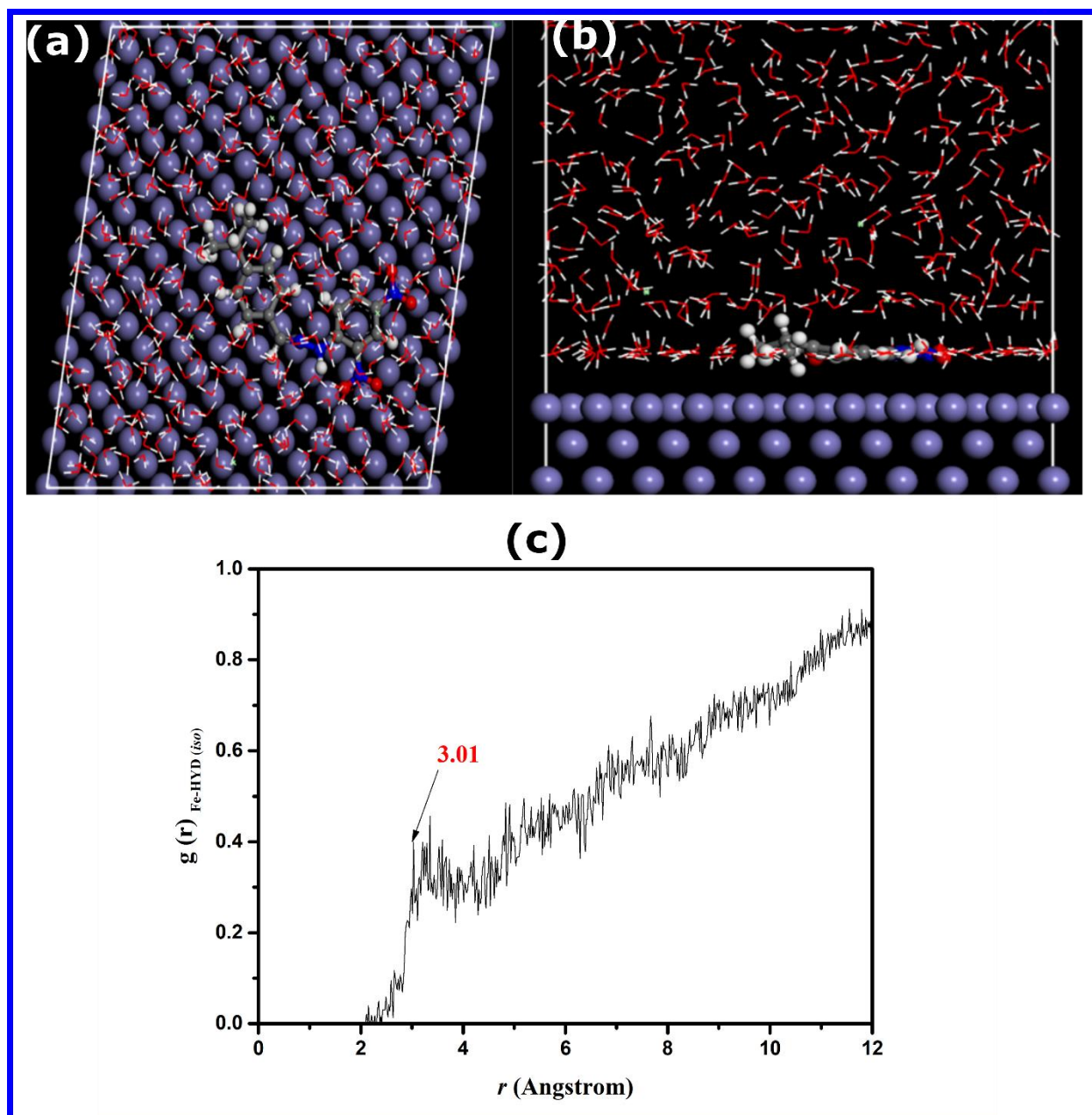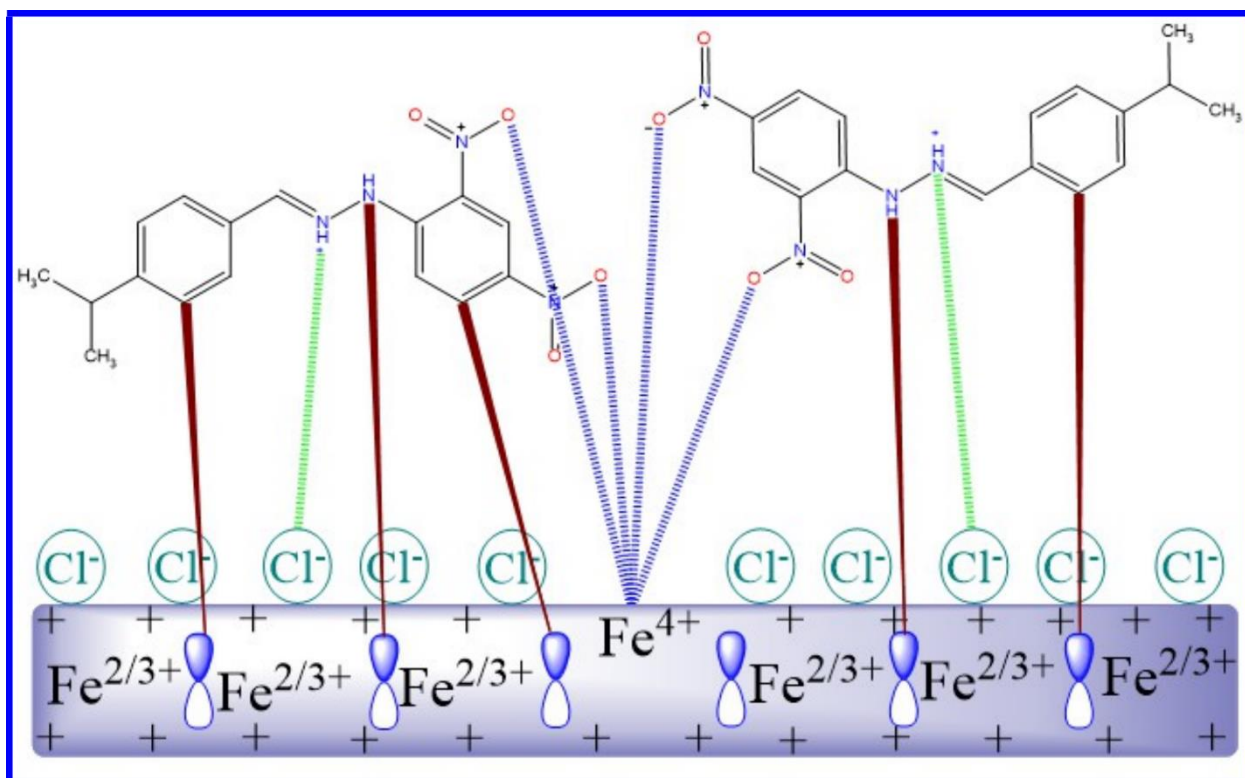
LUMO

ESP
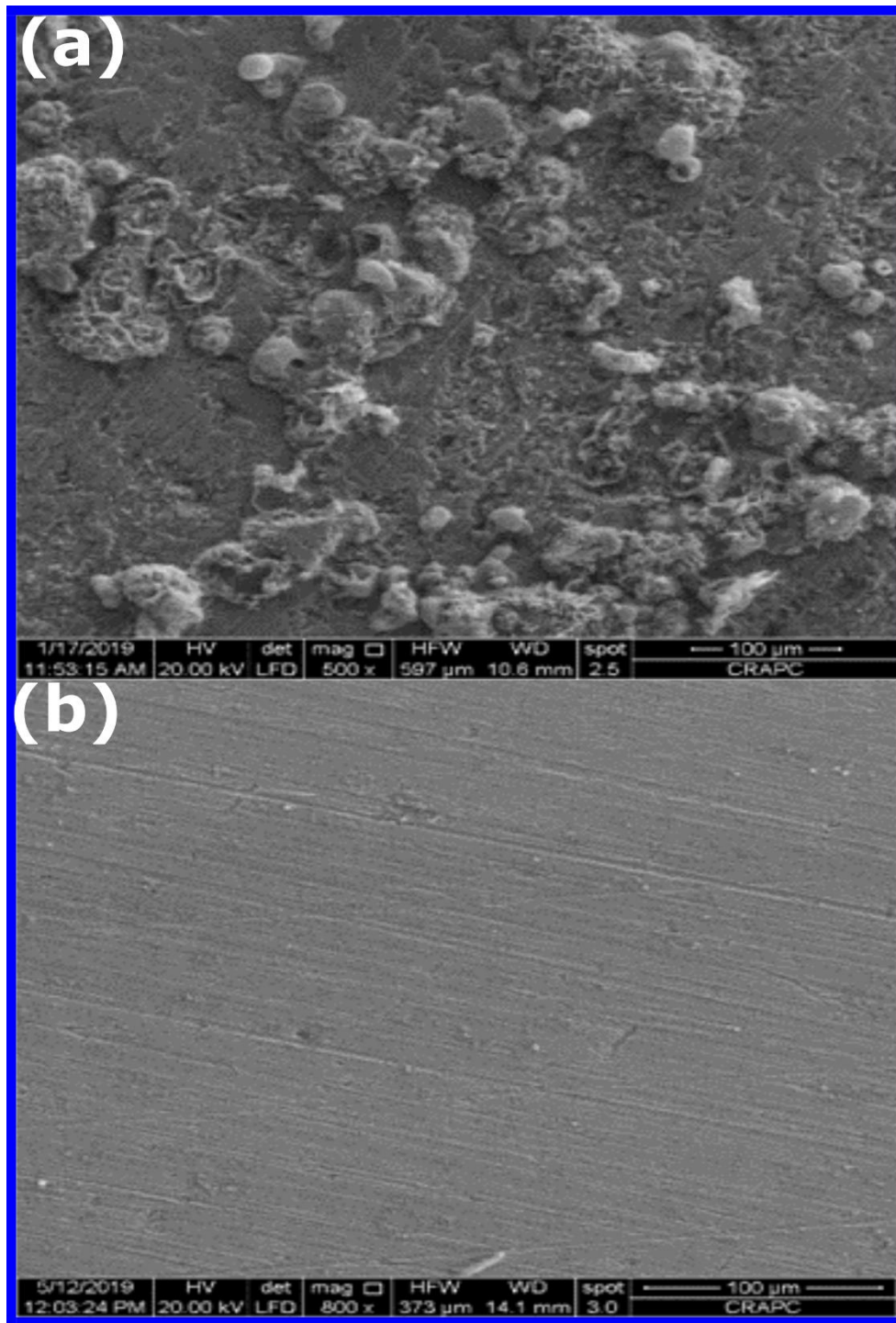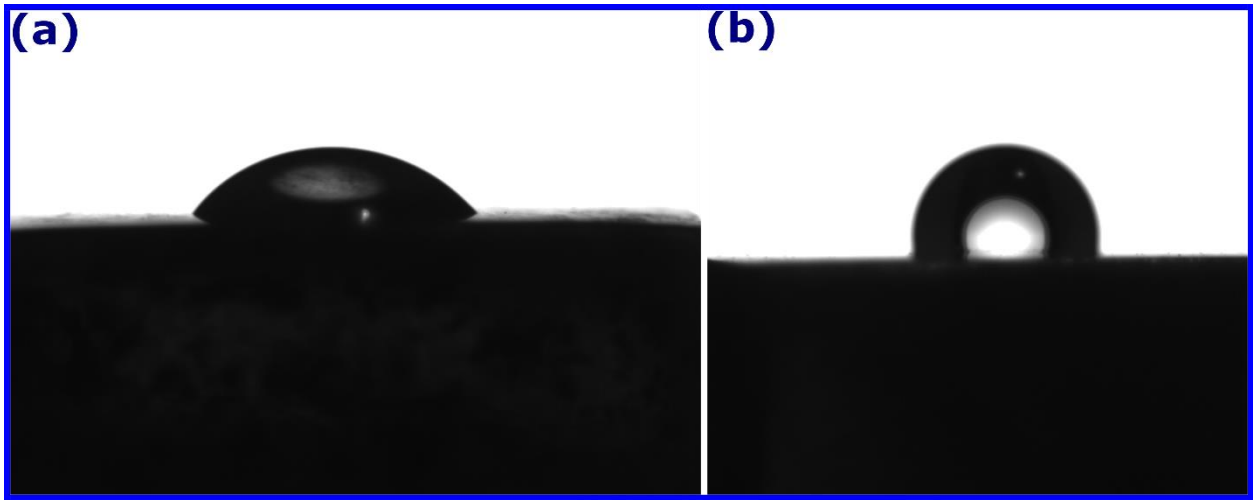
Figure 10.

Figure 11.

Author Contributions Section:

Oday Mohammad Ahmad Khamaysa, Ilhem Selatnia and Hadjer Zeghache: Performed the experiments and calculations, analyzed the data, and wrote the initial manuscript.

Hassane Lgaz, Merzoug Benahmed, Noureddine Gherraf: Contributed data or analysis tools, performed the analysis, review&editing.

Assia Sid: Performed the synthesis of compounds, review & editing.

Paul Mosset: Performed the spectroscopic analysis, review & editing.

Hassan Lgaz and Ill-Min Chung: Conceived and designed the analysis, supervision, formal analysis, review&editing

41

Conflict of interest:

The authors declare that they have no known competing financial interests or personal relationships that could have appeared to influence the work reported in this paper.

Graphical abstract
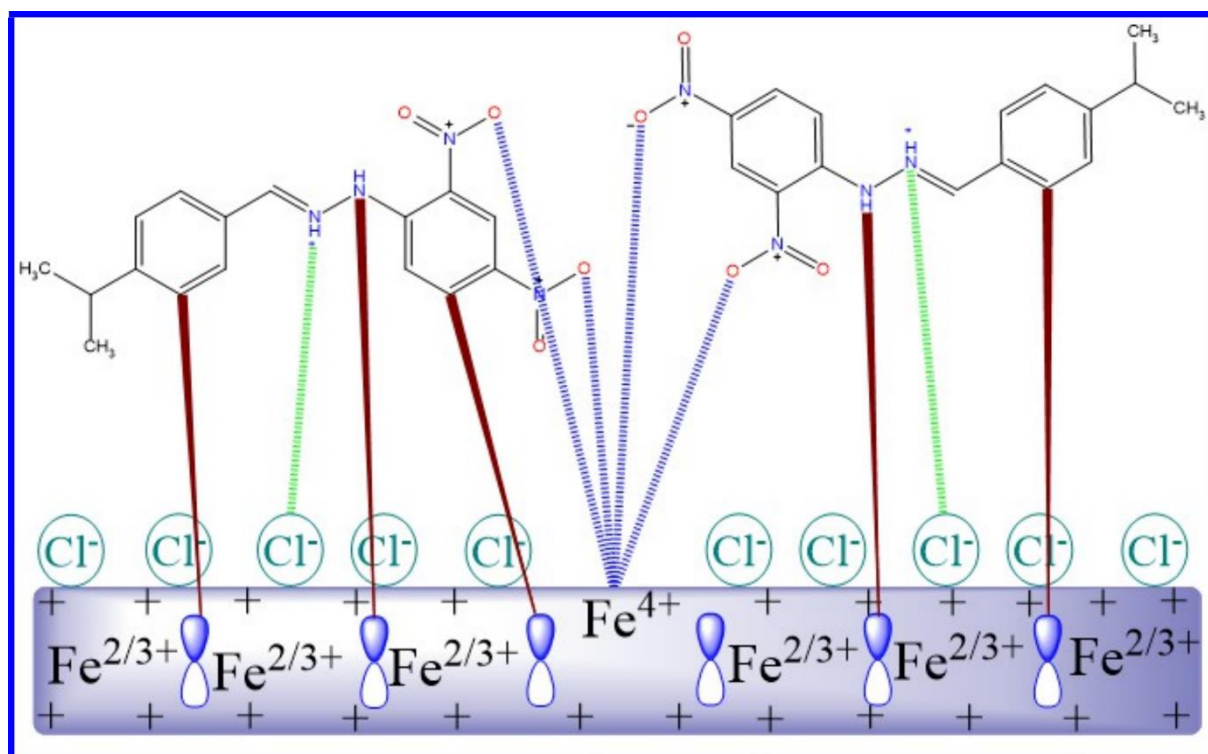
Highlights

- New synthetized hydrazone derivative acted as an efficient corrosion inhibitor.

- NO_2 groups are the most basic active site.

- XPS results confirmed the formation of an oxoiron (IV) complex.

- The hydrazone derivative acted as mixed type inhibitor.

- MD simulation confirm the adsorption of the hydrazone on the metal surface.